Journal of Dental Sciences 19 (2024) 1004–1011

Available online at www.sciencedirect.com

ScienceDirect

journal homepage: www.e-jds.com

Original Article

Volumetric analysis of artifacts from fiducial markers under cone beam computed tomography

Hsin-Yu Kuo [a], Kuan-Ling Lin [b], Ching-Ying Hsu [b], Po-Sung Fu [c,d], Chun-Cheng Hung [c,d*], Seung Jun Song [e**]

[a] School of Dentistry, Chung Shan Medical University, Taichung, Taiwan
[b] Division of Prosthodontics, Department of Dentistry, Taipei Medical University Hospital, Taipei, Taiwan
[c] Department of Dentistry, Kaohsiung Medical University Hospital, Kaohsiung, Taiwan
[d] School of Dentistry, College of Dental Medicine, Kaohsiung Medical University, Kaohsiung, Taiwan
[e] Division of Prosthodontics, College of Dental Medicine, Columbia University, New York, USA

Received 11 June 2023; Final revision received 30 June 2023
Available online 16 July 2023

KEYWORDS
Fiducial markers;
CBCT;
Volumetric analysis;
Artifacts;
Alignment

Abstract *Background/purpose:* Computer aided implant surgery has been widely adopted in modern implant dentistry. However, absence of reliable anatomic landmarks for superimposing digital data sets for patients with terminal dentition or complete edentulism remained challenging. Utilization of additional fiducial markers intraorally as the reference points for the improvement of accuracy became crucial in implant digital workflow. Nevertheless, the choice of the material for fiducial markers should present the least radiographic artifacts under cone beam computed tomography (CBCT) for better accuracy. The aim of this in vitro study was to investigate the volume of radiographic artifacts generated through different materials under the image of CBCT.

Materials and methods: Fifteen dental materials were selected and configured into cubic shape. All the materials were scanned initially with the laboratory scanner as the control groups. The samples were scanned by CBCT machine as test groups and the volume of artifact generated under CBCT images were compared and analyzed using 3D modeling software.

Results: Eleven out of fifteen materials could be recognized under CBCT images. Volumetric analysis reported that statistically significant differences among the materials could be noted, and the flowable composite resin presented the least volumetric difference. Lithium disilicate glass-ceramic, flowable composite resin, and gutta-percha presented the least deformation and maintained their cubic shapes.

* Corresponding author. School of Dentistry, College of Dental Medicine, Kaohsiung Medical University, No. 100, Shih-Chuan 1st Road, Kaohsiung, 80756, Taiwan.
** Corresponding author. Division of Prosthodontics, College of Dental Medicine, Columbia University, 622 W 168th Street, PH-7-314, New York, NY 10032, USA.
E-mail addresses: chuchh@kmu.edu.tw (C.-C. Hung), ss5080@cumc.columbia.edu (S.J. Song).

https://doi.org/10.1016/j.jds.2023.07.001

Conclusion: The results of the present study may imply that flowable composite resin compared to all ceramic materials, amalgam and gutta-percha may be a preferable choice when utilized as fiducial markers under CBCT images.

Introduction

Development in computer aided implant surgery has facilitated prosthetically driven implant placement.[1] Such surgical approach utilizes pre-operatively planned templates customized to the patient's anatomy. Adequate three-dimensional (3D) placement of a dental implant is a prerequisite for successful implant therapy.[2]

Digital workflow starts with obtaining accurate digitized scans of the patient. Alignment of such multiple datasets has allowed 3D virtual surgical planning. In cone beam computed tomography (CBCT) imaging, delineation of the dentition and soft tissue is still arduous. For that purpose, alignment of multiple datasets such as standard tessellation language (STL) of surface scanning data representing the patient's oral environment and digital imaging communication of medicine (DICOM) files from CBCT images is a necessity. For dentate patients, dentition is utilized as landmarks for dataset alignment. In contrast, in the case of edentulous patients procuring an optimal alignment may prove to be challenging due to lack of reliable landmarks. Under such circumstances, utilization of adequate artificial landmarks (fiducial markers) may be beneficial for image registration of the optical intraoral scan to CBCT image. The material of choice for fiducial markers should be easy to acquire, configure and scanned intraorally yet reflecting radiopacity with minimal radiographic artifacts generated under CBCT images.[3]

CBCT imaging is a volumetric imaging technique, which the detector accumulates multiple 2D projection images at various angles to mathematically construct into a 3D image. Almost all commercially available machines utilize Feldkamp algorithm[4] either in its original form or in various modifications.[5] The Feldkamp algorithm only approximates the line integrals, one consequence is that its quality degrades with increasing detector angles.[3] This factor in combination with other insufficiencies inherent in the measurement and reconstruction process introduces artifacts into the cone beam data sets.[5] Dental materials may have different attenuation coefficients compared to bone or soft tissue.[6] Beam hardening, with scatter and noise artifacts, were reported to be the most prominent artifacts induced by high-density objects in the beam.[7] Artifacts may decrease the accuracy of alignment processes between radiographic data and surface data.[8] Nevertheless, there are limited reports in the body of the literature discussing the ideal material recommended for fiducial markers in consideration of radiopacity and relative artifacts under CBCT images.[9] To find materials that are convenient and affordable, we randomly collected materials from a dental clinic and a dental laboratory.

The primary aim of this in vitro study was to investigate radiographic artifacts generated from different fiducial markers under CBCT images.

Materials and methods

Sample preparation

Fifteen dental materials were tested and included the following: feldspar ceramic (VITABLOCS® Mark II, VITA Zahnfabrik, Bad Säckingen, Germany), lithium disilicate glass-ceramic (IPS e. max® CAD, Ivoclar Vivadent, Schaan, Liechtenstein) pre-sintered and post-sintered, zirconia-reinforced lithium silicate (ZLS) ceramic (Celtra Duo, Dentsply Sirona, York, PA, USA) pre-sintered and post-sintered, hybrid ceramic (VITA ENAMIC®, VITA Zahnfabrik, Bad Säckingen, Germany), zirconia 3Y-TZP (3D pro-Zir®, Aidite technology, Qinhuangdoo, China), polymethyl methacrylate (PMMA) (Ceramill® temp, Amann Girrbach North America, Charlotte, NC, USA), bis-acrylic composite (Protemp™ 4, 3 M, Saint Paul, MN, USA), packable composite resin (Grandio, VOCO Gmbh, Cuxhaven, Germany), and flowable composite resin (Grandio Flow, VOCO Gmbh, Cuxhaven, Germany), gutta-percha (Obtura Flow 150®, Obtura Spartan Endodontics, Algonquin, Il, USA), glass ionomer composite liner (Ionoseal®, VOCO America, Indian Land, SC, USA), resin-modified glass ionomer restorative (Fuji II LC®, GC America, Alsip, IL, USA), amalgam (Permite, SDI Limited, Victoria, Australia). Each material was configured into 2 × 2x2 mm cubes (Figs. 1 and 2).

Dental laboratory scan and radiographic scan

First, materials were scanned with a laboratory scanner (D2000, 3Shape Copenhagen, Denmark). To reduce light reflection during scanning, each material was sprayed with scan powder (Denu Easy Scan Propellant powder spray, HDI, Ulsan, South Korea) before scanning. Digital cube models were exported as STL files and noted as the reference model (RM) (Fig. 3).

Second, the materials were positioned using wax with a 10 mm distance between each material to avoid interference of images and were scanned with a CBCT machine (Planmeca ProMax® 3D Classic, Planmeca, Helsinki, Finland) (Fig. 4).

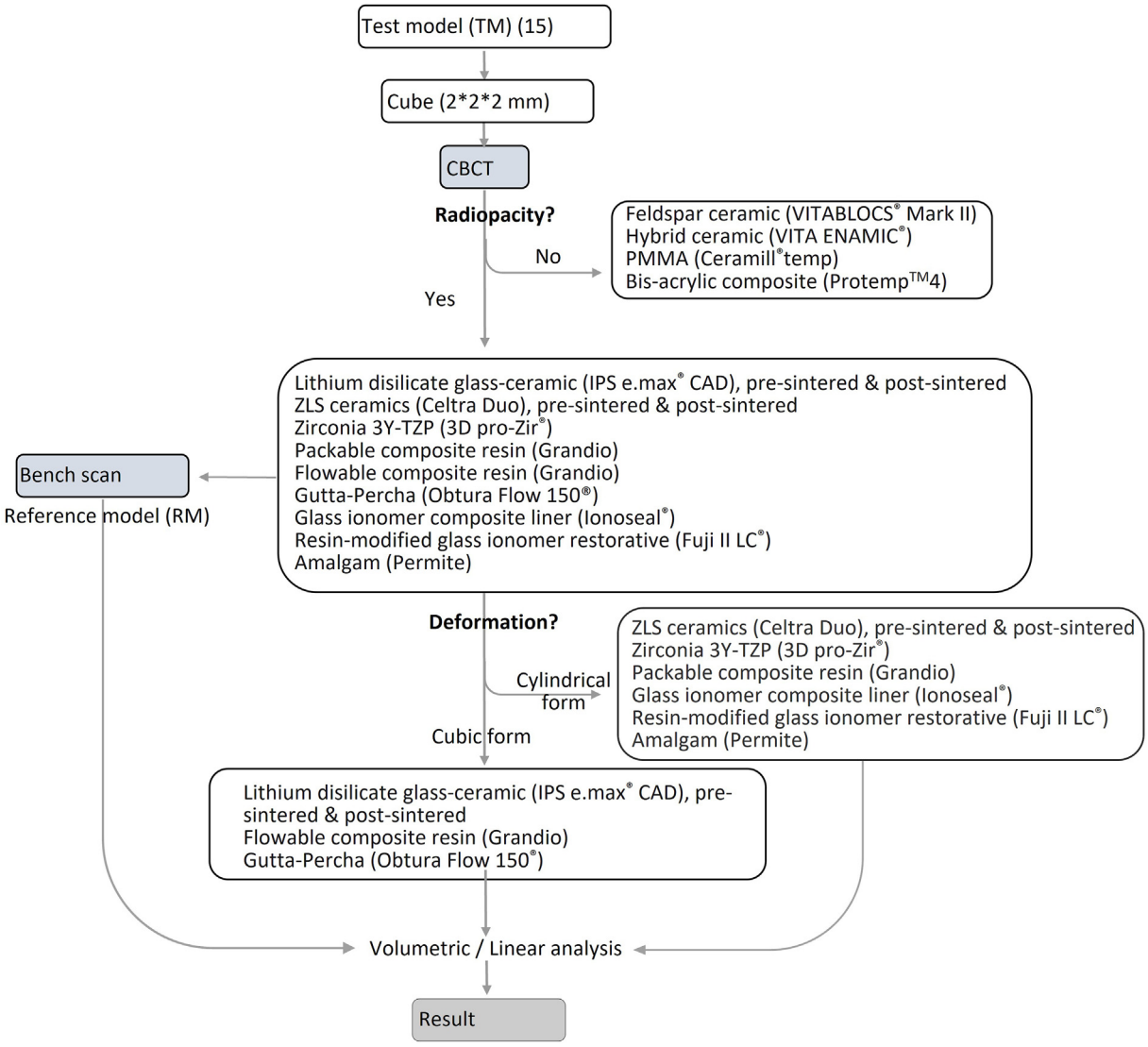

Fig. 1 Complete workflow of the testing process.

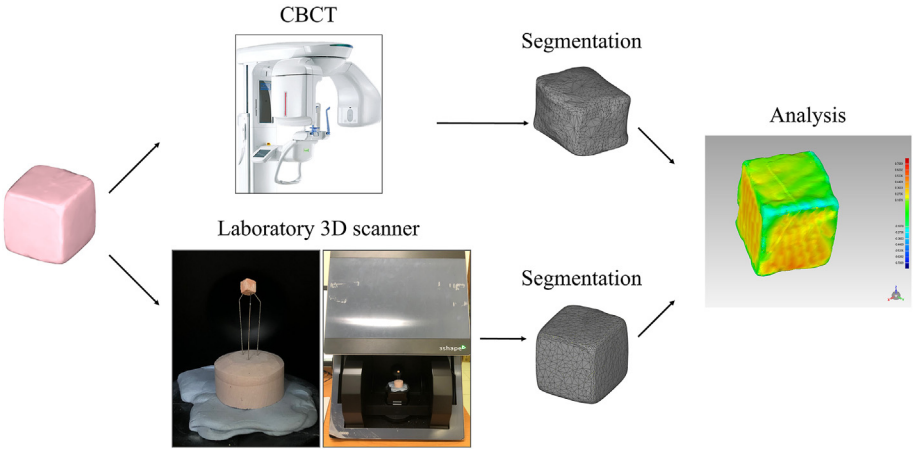

Fig. 2 A simplified version of the testing process.

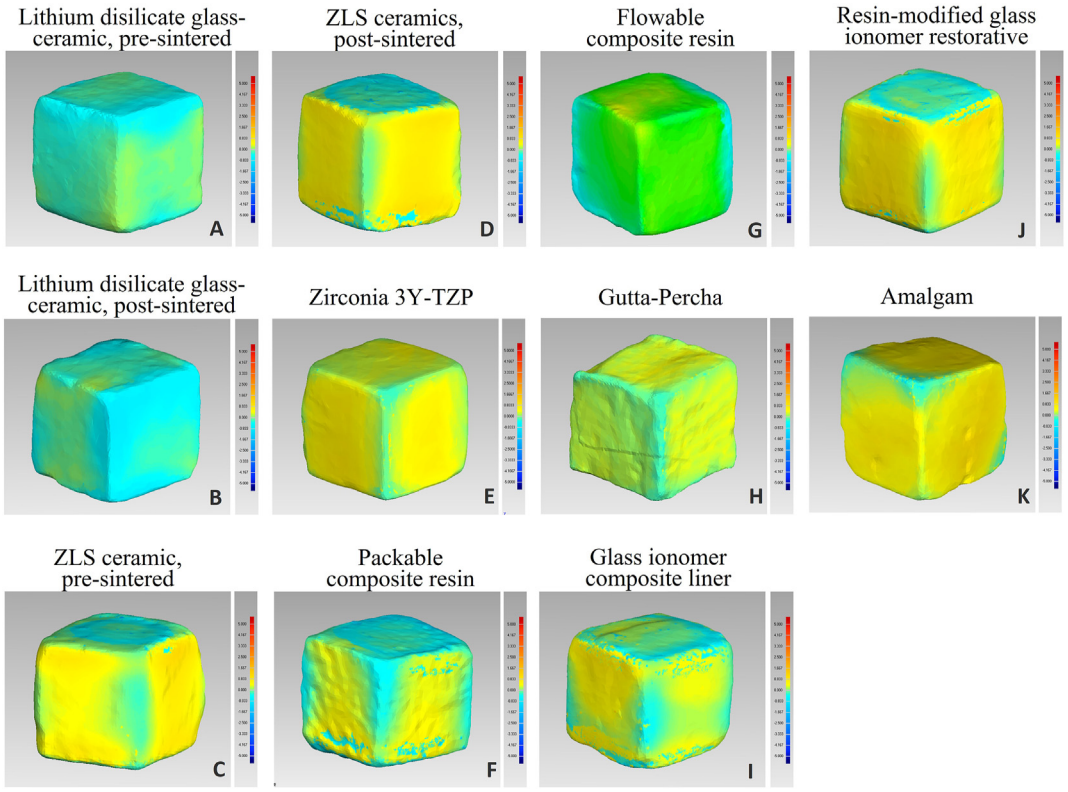

Fig. 3 Reference model (RM) exported with a laboratory scanner. (A) Lithium disilicate glass-ceramic (IPS e.max® CAD), pre-sintered. (B) Lithium disilicate glass-ceramic (IPS e.max® CAD), post-sintered. (C) ZLS ceramics (Celtra Duo), pre-sintered. (D) ZLS ceramics (Celtra Duo), post-sintered. (E) Zirconia 3Y-TZP (3D pro-Zir®). (F) Packable composite resin (Grandio). (G) Flowable composite resin (Grandio). (H) Gutta-percha (Obtura Flow 150®). (I) Glass ionomer composite liner (Ionoseal®). (J) Resin-modified glass ionomer restorative (Fuji II LC®). (K) Amalgam (Permite).

Exposure parameters for the machine setup were 84 kV, 8 mA, Ø80 × 80 mm volume size, and 75 μm isotropic voxel size. According to the manufacturer's recommendations, these settings may reduce noise around objects in CBCT images. CBCT scans were repeated 4 times. The DICOM datasets were imported into a 3D analysis software (Osirix MD 12.0, Pixmeo, Geneva, Switzerland). Segmentation of the image was performed using the segmentation toolset available in the software. The value of the threshold was selected based upon a local gray scale (voxel value) and image gradient. The intensity of the gradient was adjusted to achieve optimal value of the threshold representing well-defined outline of the cubic structure (range 1000–1200). The image was specified along the outline and was isolated from the background for the calculation of volume. The DICOM files were converted to STL files and specified as test model (TM) (Fig. 5).

Data registration and surface difference calibration (volumetric analysis)

The volume of each material was calculated using 3D modeling software (Geomagic control X, 3D Systems, Rock Hill, SC, USA). The differences between the RM and TM were calculated as (TM-RM)/RM x 100%. Furthermore, the two data sets (TM and RM) were aligned and volumetric analysis was performed with iterative closest point (ICP) algorithm[10] using a 3D modeling software (Geomagic control X, 3D Systems). The deformation of fiducial material under CBCT images were analyzed using the following comparison metrics: Root mean square error (RMSE $= \sqrt{(f - o^2)}$ whereas f is forecasts (expected values or unknown results) and o is observed values (known results)) and maximum error that calibrate the mean and maximum distance between the two surfaces at anatomically corresponding locations. In addition, the mean and the standard deviation of the calculated distances between the different points on the surface of each model were generated and expressed as a color-coded visualization map. Lastly, the software output provided the minimum, maximum, and median (first quartile and third quartile) for the surface distances.

Statistical analysis

Statistical analysis was carried out with analytics software (IBM® SPSS® Statistics 22, IBM, Armonk, NY, USA). Trueness was calculated by using the comparison among each tested group. The comparison between RM and TM for the volumetric analysis and deformation was performed using Kruskal–Wallis analysis. The P value was corrected using the Bonferroni method and the significance level was set at $P < 0.05$.

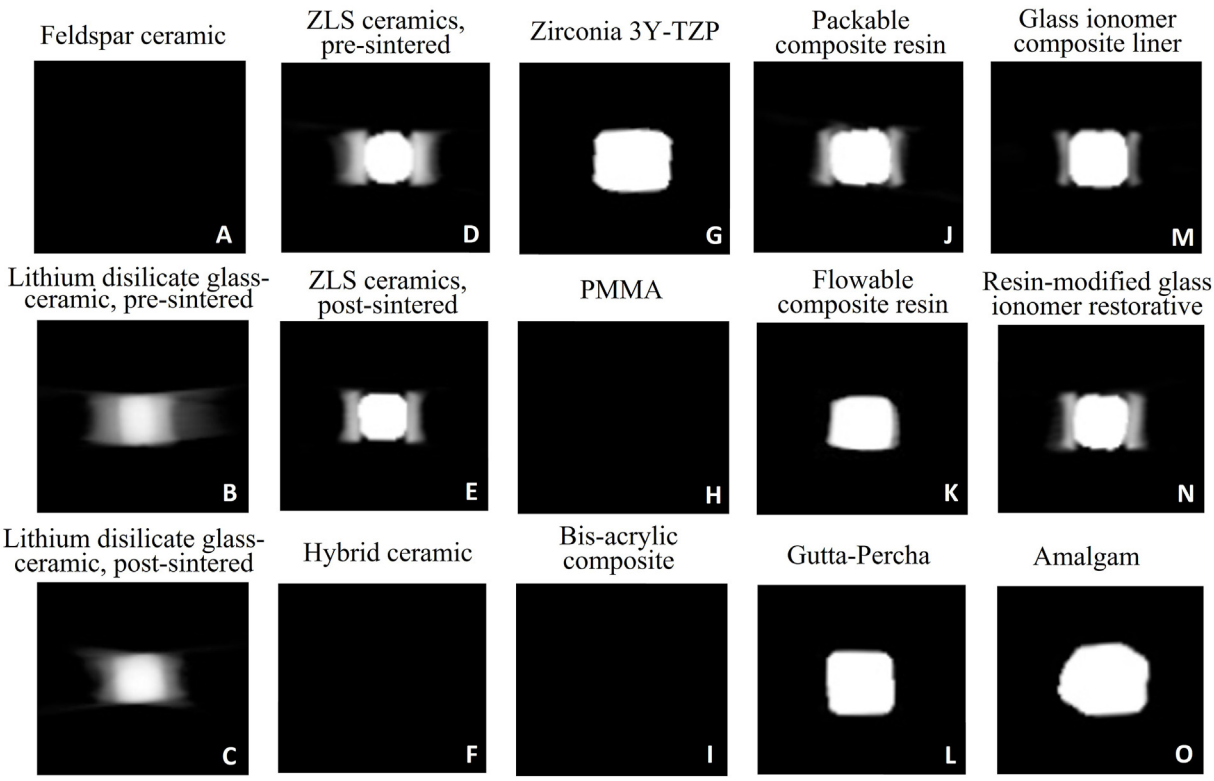

Fig. 4 The materials were scanned with a CBCT machine. (A) Feldspar ceramic (VITABLOCS® Mark II). (B) Lithium disilicate glass-ceramic (IPS e.max® CAD), pre-sintered. (C) Lithium disilicate glass-ceramic (IPS e.max® CAD), post-sintered. (D) ZLS ceramics (Celtra Duo), pre-sintered. (E) ZLS ceramics (Celtra Duo), post-sintered. (F) Hybrid ceramic (VITA ENAMIC®). (G) Zirconia 3Y-TZP (3D pro-Zir®). (H) PMMA (Ceramill®temp). (I) Bis-acrylic composite (Protemp™ 4). (J) Packable composite resin (Grandio). (K) Flowable composite resin (Grandio). (L) Gutta-percha (Obtura Flow 150®). (M) Glass ionomer composite liner (Ionoseal®). (N) Resin-modified glass ionomer restorative (Fuji II LC®). (O) Amalgam (Permite)

Results

Radiopacity

A total of 15 dental materials were included in the present study. Following initial CBCT scan, the cubic samples were divided into two groups according to their respective radiopacity. Some of the materials were radiolucent and could not be recognized under CBCT images, including feldspar ceramic, hybrid ceramic, polymethyl methacrylate (PMMA), and bis-acrylic composite. The radiolucent group which lacks the characteristics for identification were eliminated from the following analysis. The remaining eleven materials categorized as radiopaque group were prepared for volumetric analysis. The radiopaque materials were: lithium disilicate glass-ceramic pre-sintered and post-sintered, zirconia-reinforced lithium silicate (ZLS) ceramic pre-sintered and post-sintered, zirconia 3Y-TZP, packable composite resin, and flowable composite resin, gutta-percha, glass ionomer composite liner, resin-modified glass ionomer restorative, amalgam.

Volumetric analysis

Three-dimensional models (RM and TM) exported from reference and test scans were morphologically compared utilizing 3D modeling software (Geomagic control X, 3D Systems). Increase of volume was noted in most of the materials when comparing RM and TM. In contrary, lithium disilicate glass-ceramic pre-sintered ($-15.3 \pm 5.7\%$) and post-sintered ($-20.8 \pm 7.4\%$) exhibited decreased volume. Flowable composite had significantly less volumetric difference compared to other materials ($P < 0.05$) ($3.8 \pm 2.1\%$). Volumetric analysis reported significant differences among the eleven materials evaluated (Table 1).

Deformation

Through the conversion of test scans to three-dimensional models (STL), it was noted that some of the materials could be recognized with their cubic form while others deformed under CBCT images and the respective models resembled a cylindrical form (Fig. 5). Four materials that maintained cubic form under CBCT images were: lithium disilicate glass-ceramic pre-sintered and post-sintered, flowable composite resin and gutta-percha. The materials that morphed into cylindrical form were: zirconia-reinforced lithium silicate (ZLS) ceramic pre-sintered and post-sintered, zirconia 3Y-TZP, packable composite resin, glass ionomer composite liner, resin-modified glass ionomer restorative, and amalgam.

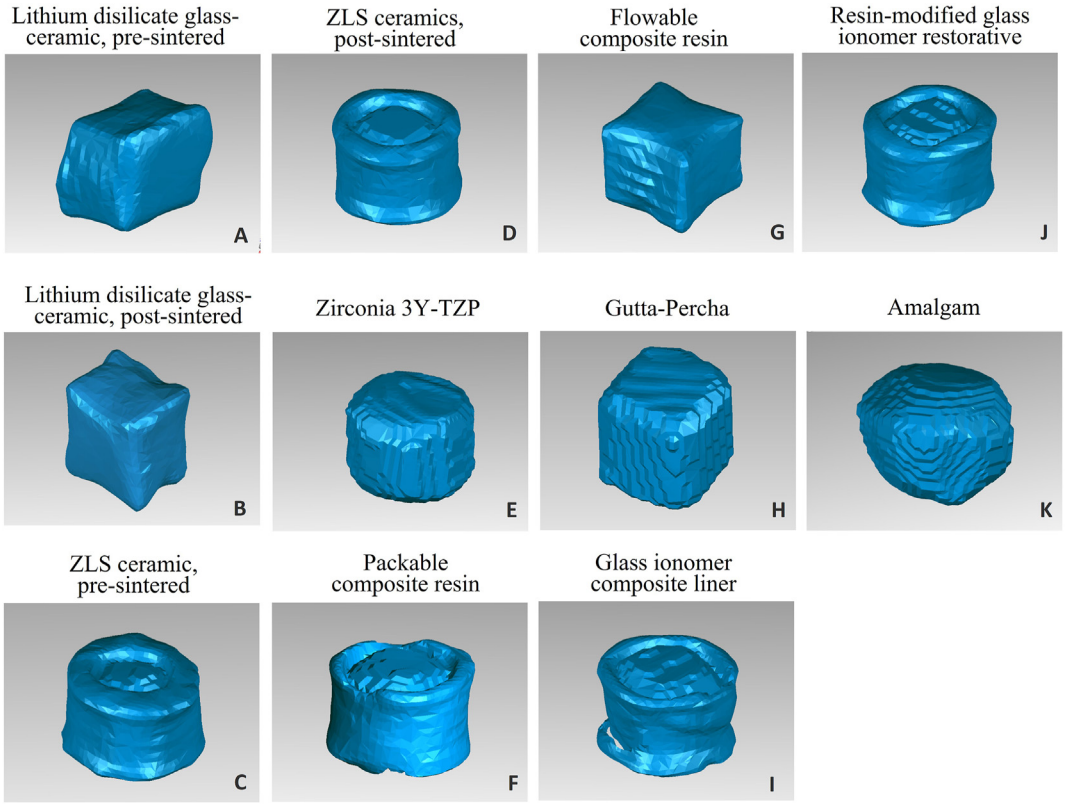

Figure 5 The DICOM files of the materials were converted to STL files and specified as test models. (A) Lithium disilicate glass-ceramic (IPS e.max® CAD), pre-sintered. (B) Lithium disilicate glass-ceramic (IPS e.max® CAD), post-sintered. (C) ZLS ceramics (Celtra Duo), pre-sintered. (D) ZLS ceramics (Celtra Duo), post-sintered. (E) Zirconia 3Y-TZP (3D pro-Zir®). (F) Packable composite resin (Grandio). (G) Flowable composite resin (Grandio). (H) Gutta-percha (Obtura Flow 150®). (I) Glass ionomer composite liner (Ionoseal®). (J) Resin-modified glass ionomer restorative (Fuji II LC®). (K) Amalgam (Permite).

All models (RM and TM) derived from reference and test scans of radiopaque materials were aligned respectively and a linear deformation analysis was performed. Models maintaining their cubic form reported smaller RMSE values compared to models deformed into cylindrical form. The results of the RMSE value showed a statistically significant difference among four cubic models ($P < 0.05$), and the RMSE values in descending order were: lithium disilicate glass-ceramic post-sintered, lithium disilicate glass-ceramic pre-sintered, gutta-percha, and flowable composite resin (Table 2).

Discussion

Advancements in digital radiographic imaging, computer aided design/computer aided manufacturing (CAD/CAM) and surgical planning software has significantly improved prosthetically driven implant planning and communication among treatment team members. To enable a virtual platform, multiple datasets representing intraoral surface and underlying anatomy needs to be aligned. Accuracy of integrating various datasets play a significant role in successful planning and placement of dental implants.

Digital radiographic imaging makes it possible to digitize and virtualize the anatomy of the patient. Following alignment with surface data, a virtual platform for surgical and prosthetic planning is enabled. Alignment is performed with ICP[10] utilizing hard tissue anatomical landmarks. For the cases which lack anatomical landmarks, fiducial markers situated on prostheses may assist in proper alignment of datasets. Minimizing artifacts due to fiducial markers in CBCT images is of importance. With better quality images, alignment of DICOM to STL may be more accurate as artifacts tend to interfere with proper alignment.[11] An American Association of Physicists in Medicine task group report stated that CT streak artifacts can be locally significant, similar interpretation can be made for CBCT images.[12]

In the present study, various dental materials that can be easily acquired from chair side and laboratory was collected. Materials were fabricated in cubic form rather than ball form for the convenience of identifying orientation. Radiopacity of the materials were determined first for suitability as fiducial markers. After removal of four samples due to radiolucency, eleven samples were further investigated for artifact analysis.

Using gray scale (voxel value) as a reference for radiopacity has been reported in various studies.[12,13] Thereby we utilized a standardized gray scale (range 1000–1200) for DICOM exportation to minimize inter-sample discrepancies.

The materials showed various amounts of artifacts and deformation in CBCT imaging. Such characteristics of material would hinder the formation of three-dimensional

Table 1 Volumetric analysis of the tested materials.

Material	Volumetric volume difference (%)	Radiologic visualization	Recognizing directionality
	Mean ± SD		
Feldspar ceramic	−100.0 ± 0.0	no	no
Lithium disilicate glass-ceramic, pre-sintered	−15.3 ± 5.7	yes	yes
Lithium disilicate glass-ceramic, post-sintered	−20.8 ± 7.4	yes	yes
ZLS ceramics, pre-sintered	26.6 ± 8.2	yes	no
ZLS ceramics, post-sintered	39.4 ± 5.6	yes	no
Hybrid ceramic	−100.0 ± 0.0	no	no
Zirconia 3Y-TZP	51.1 ± 12.9	yes	no
PMMA	−100.0 ± 0.0	no	no
Bis-acrylic composite	−100.0 ± 0.0	no	no
Packable composite resin	19.1 ± 4.7	yes	no
Flowable composite resin	3.8 ± 2.1	yes	yes
Gutta-percha	11.7 ± 3.2	yes	yes
Glass ionomer composite liner	18.1 ± 3.2	yes	no
Resin-modified glass ionomer restorative	34.2 ± 8.3	yes	no
Amalgam	76.5 ± 10.0	yes	no

ZLS, zirconia-reinforced lithium silicate; PMMA, polymethyl methacrylate; SD, standard deviation.

Table 2 Linear deformation analysis.

Material	Max (mm)	Min (mm)	RMS (mm) Mean ± SD
Lithium disilicate glass-ceramic, pre-sintered	0.24	−0.57	0.25 ± 0.13[a]
Lithium disilicate glass-ceramic, post-sintered	0.29	−1.42	0.30 ± 0.14[a]
ZLS ceramics, pre-sintered	1.46	−2.01	0.47 ± 0.41
ZLS ceramics, post-sintered	1.57	−1.99	0.53 ± 0.46
Zirconia 3Y-TZP	1.26	−1.13	0.41 ± 0.20
Packable composite resin	1.40	−2.01	0.52 ± 0.42
Flowable composite resin	0.67	−0.64	0.15 ± 0.07[a]
Gutta-percha	0.67	−0.48	0.23 ± 0.07[a]
Glass ionomer composite liner	1.41	−2.01	0.37 ± 0.35
Resin-modified glass ionomer restorative	1.13	−2.00	0.61 ± 0.45
Amalgam	1.76	−1.07	0.58 ± 0.26

ZLS, zirconia-reinforced lithium silicate; RMS, root mean square; SD, standard deviation.
[a] Statistically significant differences were obtained by the post-hoc Bonferroni test if significance at $P < 0.05$ was reached by ANOVA.

models derived from DICOM files since the outline of the images will be obscure without clear delineation. The transformation of the image from square to circular was caused by scatter (noise) under the CBCT image. Interestingly, some of the materials maintained their cubic form and others were deformed to a cylindrical form. The materials which maintained their cubic form exhibited low degree of artifacts and had advantage in the following steps of recognition and alignment of RM and TM.

Schulze et al.[5] reported noise, scatter and beam hardening as the most predominant artifacts.[5] In addition, image-degrading effect of scattered radiation will affect CBCT images more than highly-collimated CT images. Blooming artifacts have been reported to increase dental implant volumes captured in various CBCT devices by 20—30%.[14] Such blooming artifact have been attributed to the partial volume effect, motion artifacts as well as beam hardening.[15] As motion artifacts were not of an issue in the present study, majority of the blooming artifacts could be attributed to partial volume effect and beam hardening. The dental literature reports various investigations stating blooming artifacts pertaining to dental implants and associated radiographic limitations such as erroneous evaluation of dehiscence or fenestration.[14,16,17] However, comprehensive analysis in blooming effect in dental materials other than dental implants have not been extensively investigated.

Linear analysis was processed to compare the differences between RM and TM. TM with cubic form better performed in linear analysis and showed smaller RMSE values. TM with cylindrical form showed larger RMSE values which indicates greater differences between RM and TM.

The results of the study revealed that flowable composite resin presented the least amount of volumetric difference when comparing RM and TM and maintained geometric characteristics indicating that minimum amount of artifacts were generated around the subject under CBCT imaging. The investigation presents with several limitations such as usage of a single CBCT device, the lack of various exposure settings, in vitro setting, and possible inaccuracy in RM and TM superimposition due to deformation.

The present study was investigated under standardized controlled environment during CBCT scan which is independent from clinical scenarios in regards of various intraoral condition. Further investigations in regards with shape and size of fiducial markers and in vivo studies should be conducted in the future.

Declaration of competing interest

The authors have no conflicts of interest relevant to this article.

References

1. Tahmaseb A, Wu V, Wismeijer D, Coucke W, Evans C. The accuracy of static computer-aided implant surgery: a systematic review and meta-analysis. *Clin Oral Implants Res* 2018; 29(Suppl 16):S416—35.
2. Tahmaseb A, Wismeijer D, Coucke W, Derksen W. Computer technology applications in surgical implant dentistry: a systematic review. *Int J Oral Maxillofac Implants* 2014;29:25—42.
3. Iturrate M, Eguiraun H, Etxaniz O, Solaberrieta E. Accuracy analysis of complete-arch digital scans in edentulous arches when using an auxiliary geometric device. *J Prosthet Dent* 2019;121:447—54.
4. Feldkamp LA, Davis LC, Kress JW. Practical cone-beam algorithm. *J Opt Soc Am A* 1984;1:612—9.
5. Schulze R, Heil U, Gross D, et al. Artefacts in CBCT: a review. *Dentomaxillofacial Radiol* 2011;40:265—73.
6. Zhang Y, Zhang L, Zhu XR, Lee AK, Chambers M, Dong L. Reducing metal artifacts in cone-beam CT images by preprocessing projection data. *Int J Radiat Oncol Biol Phys* 2007; 67:924—32.
7. De Man B, Nuyts J, Dupont P, Marchal G, Suetens P. Metal streak artifacts in X-ray computed tomography: a simulation study. In: *IEEE nuclear science symposium and medical imaging conference*; 1998 (Cat. No. 98CH36255).
8. Valiyaparambil JV, Yamany I, Ortiz D, et al. Bone quality evaluation: comparison of cone beam computed tomography and subjective surgical assessment. *Int J Oral Maxillofac Implants* 2012;27:1271—7.
9. Choi JH, Kim Y, Yi TK, Jung J, Kim Y, Park S. Optimized marker for template-guided intraoral surgery. *Stud Health Technol Inf* 2013;184:85—91.
10. Besl P, McKay ND. A method for registration of 3-D shapes. *IEEE Trans Pattern Anal Mach Intell* 1992;14:239—56.
11. Kim JE, Park YB, Shim JS, Moon HS. The impact of metal artifacts within cone beam computed tomography data on the accuracy of computer-based implant surgery: an in vitro study. *Int J Oral Maxillofac Implants* 2019;34:585—94.
12. Papanikolaou N, Battista JJ, Boyer AL, et al. *Tissue inhomogeneity corrections for megavoltage photon beams*. Florida: Medical Physics Publishing, 2004.
13. Razi T, Niknami M, Alavi Ghazani F. Relationship between hounsfield unit in CT scan and gray scale in CBCT. *J Dent Res Dent Clin Dent Prospects* 2014;8:107—10.
14. Wanderley VA, de Faria Vasconcelos K, Leite AF, et al. Impact of the blooming artefact on dental implant dimensions in 13 cone-beam computed tomography devices. *Int J Implant Dent* 2021;7:67.
15. Pack JD, Xu M, Wang G, Baskaran L, Min J, De Man B. Cardiac CT blooming artifacts: clinical significance, root causes and potential solutions. *Vis Comput Ind Biomed Art* 2022;5:29.
16. Tarce M, de Greef A, Lahoud P, de Faria Vasconcelos K, Jacobs R, Quirynen M. The impact of implant-related characteristics on dental implant blooming: an in vitro study. *Clin Oral Implants Res* 2022;33:1199—211.
17. Costa JA, Mendes JM, Salazar F, Pacheco JJ, Rompante P, Câmara MI. Analysis of peri-implant bone defects by using cone beam computed tomography (CBCT): an integrative review. *Oral Radiol* 2023;39:455—66.